Supplementary information

The C-terminal helix of ribosomal P stalk recognizes a hydrophobic groove of elongation factor 2 in a novel fashion

Takehito Tanzawa[1], Koji Kato[1,2], Dylan Girodat[3], Toyoyuki Ose[1,2], Yuki Kumakura[1], Hans-Joachim Wieden[3], Toshio Uchiumi[4], Isao Tanaka[2] and Min Yao[1,2,*]

[1]Graduate School of Life Science, Hokkaido University, Sapporo, Hokkaido, 060-0810 Japan

[2]Faculty of Advanced Life Science, Hokkaido University, Sapporo, Hokkaido, 060-0810 Japan

[3]Alberta RNA Research and Training Institute, Department of Chemistry and Biochemistry, University of Lethbridge, Lethbridge, AB T1K 3M4, Canada.

[4]Department of Biology, Faculty of Science, Niigata University, 8050 Ikarashi 2-no-cho, Nishi-ku, Niigata 950-2181, Japan

[*]To whom correspondence should be addressed. Tel: +81-11-706-4481, Fax: +81-11-706-4481, Email: yao@castor.sci.hokudai.ac.jp

Table S1. The list of *Pho*EF-2 mutants for binding assays.

Construct	Residue	Domain	Function	Mutation	Interaction
*Pho*EF-2-GMPPCP	Pro164	Domain G	P1-binding	P164S	++
	Met167			M167S	+
	Met168			M168S	++
	Phe171			F171S	++
	Val198			V198S	++
	Phe205			F205S	+
	Leu214	Subdomain G'		L214S-V216S	++
	Val216				
	Met219			M219S	++
	Lys225			K225S	++
	Phe226			F226S	-
	Asn227			N227S	++

++: The binding ability is comparable to wild type.

+: The binding ability is less similar to the wild type.

–: The binding ability is undetectable.

Table S2. Data collection and refinement statistics

	***Pho*EF-2-GMPPCP/-apo**	***Pho*EF-2-D2-GDP**	***Pho*EF-2-GMPPCP-P1C11**
PDB ID	5H7J	5H7K	5H7L
Data Collection			
Beamline	PF AR-NW12A	PF BL-5A	SPring-8 BL44XU
Wavelength (Å)	1.0000	1.0000	1.0000
Resolution range (Å)	39.59–2.30 (2.44–2.30)[a]	47.56–1.60 (1.70–1.60)	48.43–3.10 (3.27–3.10)
Space group	$P2_12_12_1$	$P2_12_12_1$	$P2_12_12_1$
Unit-cell parameters (Å)	a = 84.2 b = 116.1 c = 189.2	a = 50.2 b = 85.6 c = 114.4	a = 79.8 b = 121.9 c = 199.3
Completeness (%)	99.2 (98.7)	99.9 (99.7)	99.0 (98.0)
Redundancy	5.14 (5.15)	7.25 (7.24)	5.75 (5.72)
Average I/σ(I)	20.23 (3.80)	19.07 (2.52)	15.69 (2.86)
R_{merge}[b]	0.05 (0.389)	0.077 (0.729)	0.07 (0.598)
Molecules/ asymmetric unit	2	1	2
Refinement			
R_{work}/R_{free} (%)[c]	21.51/25.67	17.12/19.79	23.02/28.54
Atoms			
Amino acid residues	10880	3003	11052
Water molecules	205	408	0
Ligands	32	28	64
RMSD from ideality			
Bond length (Å)	0.010	0.007	0.011
Torsion angle (°)	1.320	1.131	1.644
Ramachandran plot (%)			
Favoured	96.85	98.67	93.59
Allowed	2.49	1.33	6.12
Outliers	0.66	0.00	0.29

[a]Values in parentheses are for the highest resolution shell.

[b]$R_{merge} = \sum_{hkl}\sum_i|I_i(hkl)-\langle I_i(hkl)\rangle|/\sum_{hkl}\sum_i I_i(hkl)$, where i is the number of observations of a given reflection and $I(hkl)$ is the average intensity of the i observations. R_{free} was calculated with a 5% fraction of randomly selected reflections evaluated from refinement. The highest resolution shell is shown in parentheses.

[c]$R_{work} = \sum_{hkl}||F_{obs}|-|F_{calc}||/\sum_{hkl}|F_{obs}|$, R_{free} was calculated for 5% randomly selected test sets that were not used in the refinement.

Figure S1

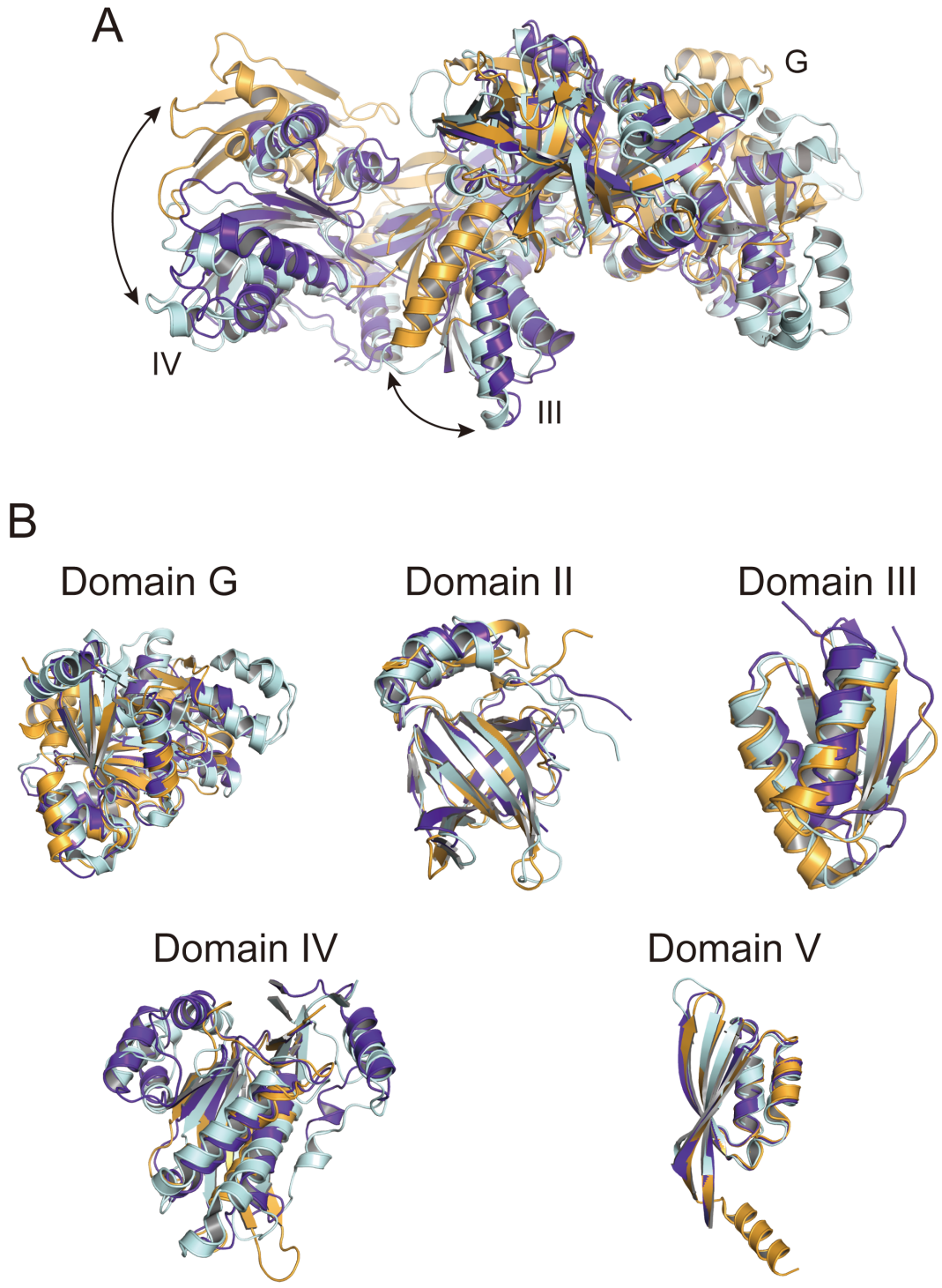

Figure S1. Structural comparison of each domain G-V among EF-2 and EF-G. (**A**) Structural comparison of *Pho*EF-2 (blue), *Sce*EF-2 (PDBID: 1N0V (pale cyan)) and *Sau*EF-G from *Staphylococcus aureus* (PDBID: 1ELO (yellow)) by superposing domain G. (**B**) Structural superposition of domains G–V among *Pho*EF-2, *Sce*EF-2, and *Sau*EF-G. Each of domains G, II, III, IV, and V of *Pho*EF-2 (blue), *Sce*EF-2 (pale cyan), and *Sau*EF-G (yellow) were superposed separately.

Figure S2

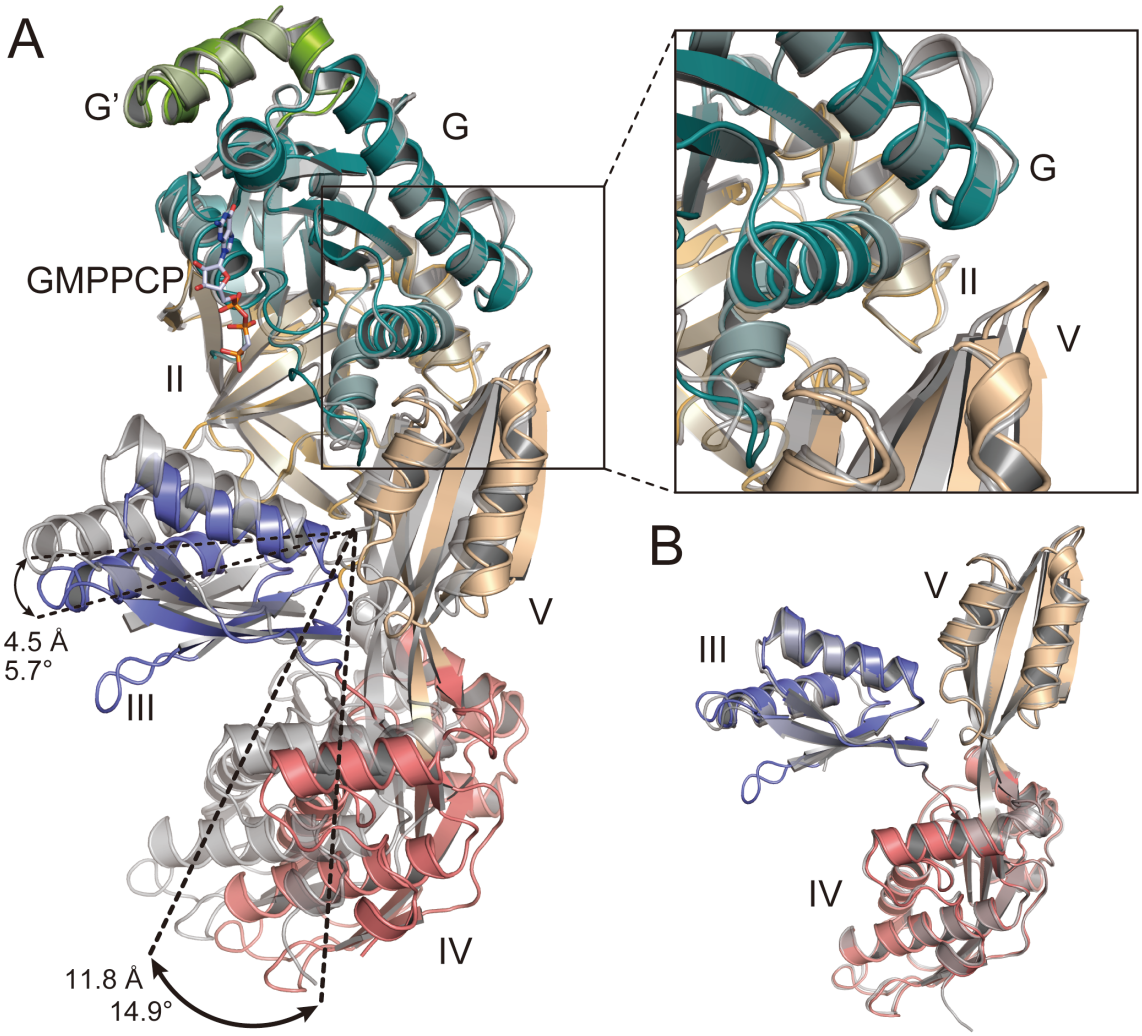

Figure S2. Structural comparison between *Pho*EF-2-Apo and *Pho*EF-2-GMPPCP. *Pho*EF-2-Apo is colored gray and *Pho*EF-2-GMPPCP is shown in the same colors as in Figure 1A. (**A**) The two structures superposed using domain G. (**B**) Structural superposition of domains III–V.

Figure S3

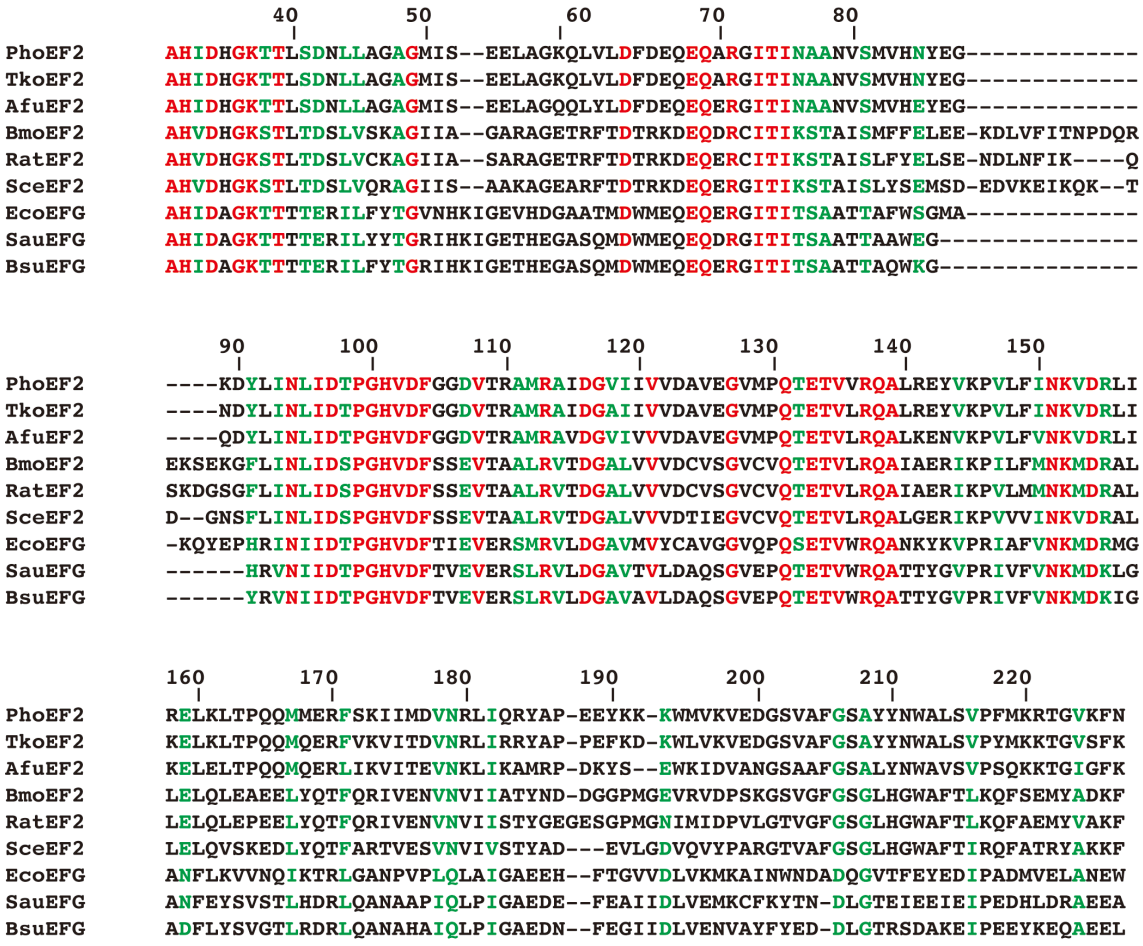

Figure S3. Sequence alignments of the GTP binding site among aEF-2, eEF-2, and EF-G. The sequences around GTP binding sites were compared: aEF-2 from *Pyrococcus horikoshii* (Pho), *Thermococcus kodakarensis* (Tko), and *Archaeoglobus fulgidus* (Afu); eEF-2 from *Bombyx mori* (Bmo), *Rattus norvegicus* (Rat), and *Saccharomyces cerevisiae* (Sce); EF-G from *Escherichia coli* (Eco), *Staphylococcus aureus* (Sau), and *Bacillus subtilis* (Bsu). Completely identical amino acids among aEF-2, eEF-2, and EF-G are colored red, while those with a conserved change are colored green.

Figure S4

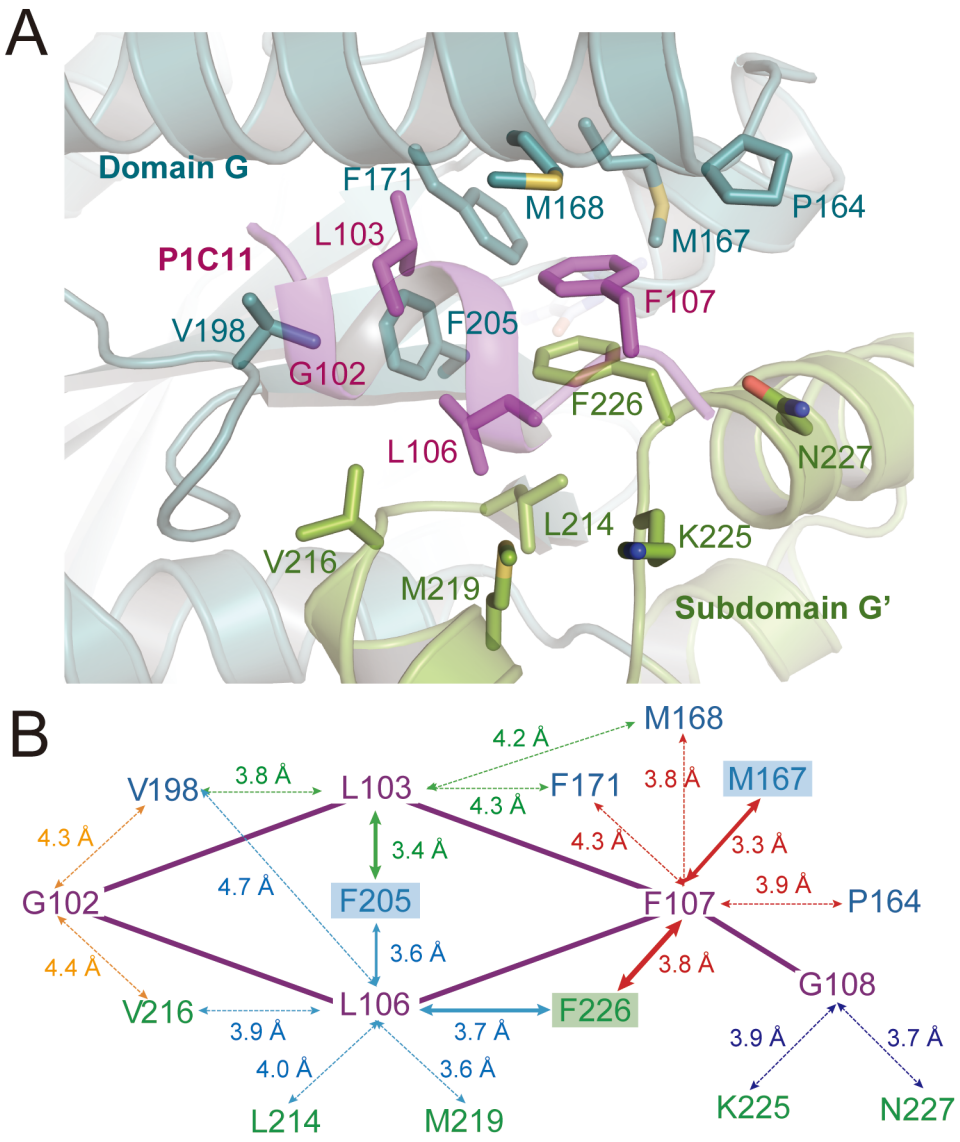

Figure S4. Structural details of the interaction between *Pho*EF-2 and P1. (**A**) Close-up view of the structure of the P1C11-binding groove. The side chains of residues of P1C11 and *Pho*EF-2 that are involved in the interaction are represented by stick models. The S atoms are colored yellow. *Pho*EF-2 and P1C11 are colored in the same way as in Figure 3. The residue G102 of P1C11 contacted residues V198 (domain G) and V216 (subdomain G′) of *Pho*EF-2. The residue L103 of P1C11 interacted with residues M168, F171, V198, and F205 (domain G). The residue L106 of P1C11 interacted with residues

V198 and F205 (domain G), and residues L214, V216, M219, and F226 (subdomain G′). Finally, residue F107 bound to residues P164, M167, M168, and F171 (domain G), and residue F226 (subdomain G′). (**B**) Schematic overview of the interaction between P1C11 and *Pho*EF-2. The color-coding of labels is the same as in (**A**). The distances are labeled and dashed-arrows indicate the stacking interactions.

Figure S5

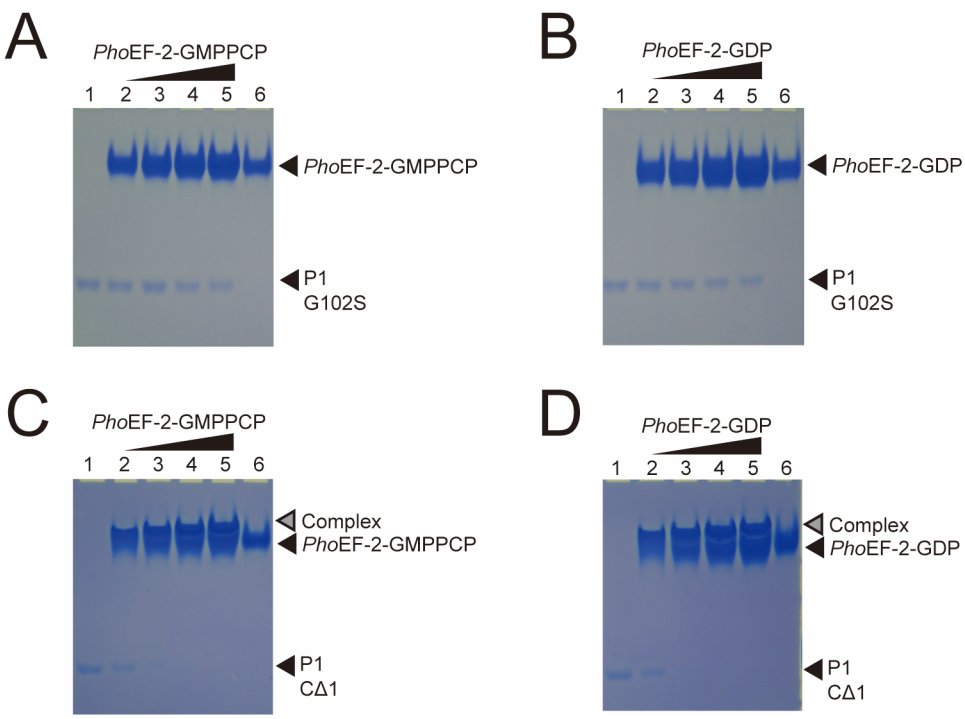

Figure S5. Binding assay of GMPPCP- and GDP-bound *Pho*EF-2 vs P1 mutants using Native-PAGE. (**A**)–(**B**) Binding assays between *Pho*EF-2-GMPPCP or *Pho*EF-2-GDP and the P1 mutant G102S. (**C**)–(**D**) Binding assays between *Pho*EF-2-GMPPCP or *Pho*EF-2-GDP and the P1 truncated mutant CΔ1 which deleted C-terminal residue G108. Each mutant of P1 homodimer (100 pmol) was incubated without *Pho*EF-2 (lane 1), or with 100 pmol (lane 2), 200 pmol (lane 3), 300 pmol (lane 4), or 400 pmol (lane 5) of the *Pho*EF-2 in a 10 μL solution at 70 °C. *Pho*EF-2 (100 pmol) was also incubated without each P1 mutant (lane 6).

Figure S6

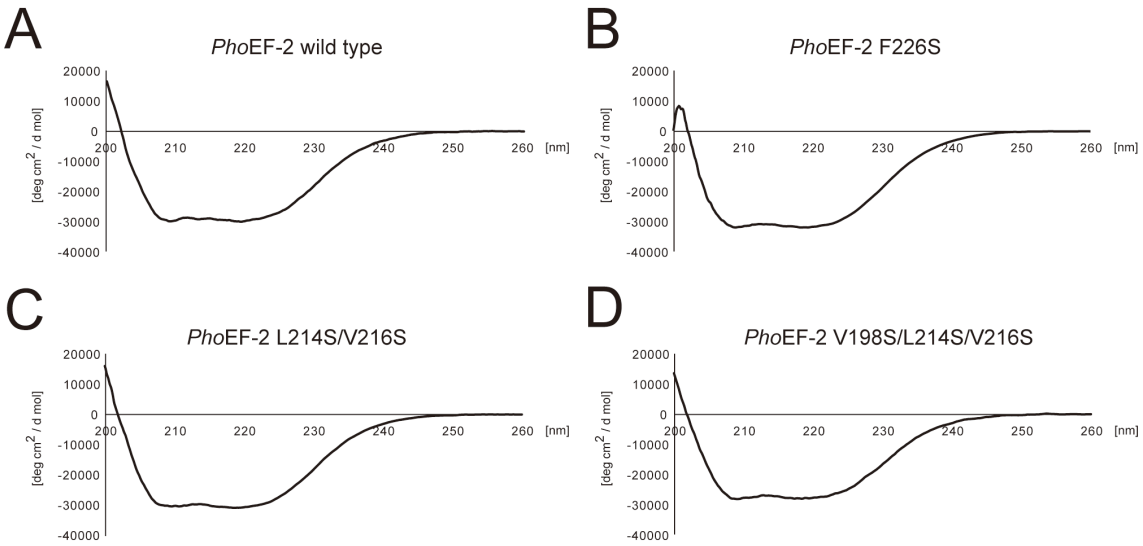

Figure S6. CD spectrometry of wild type and mutants of *Pho*EF-2. (**A**)–(**D**) are spectrometry of *Pho*EF-2 and its mutants F226S, L214S-V216S, and V198S-L214S-V216S, respectively. All CD spectrometry of them are almost similar, indicated no significant conformational changes between *Pho*EF-2 and its mutants.

Figure S7

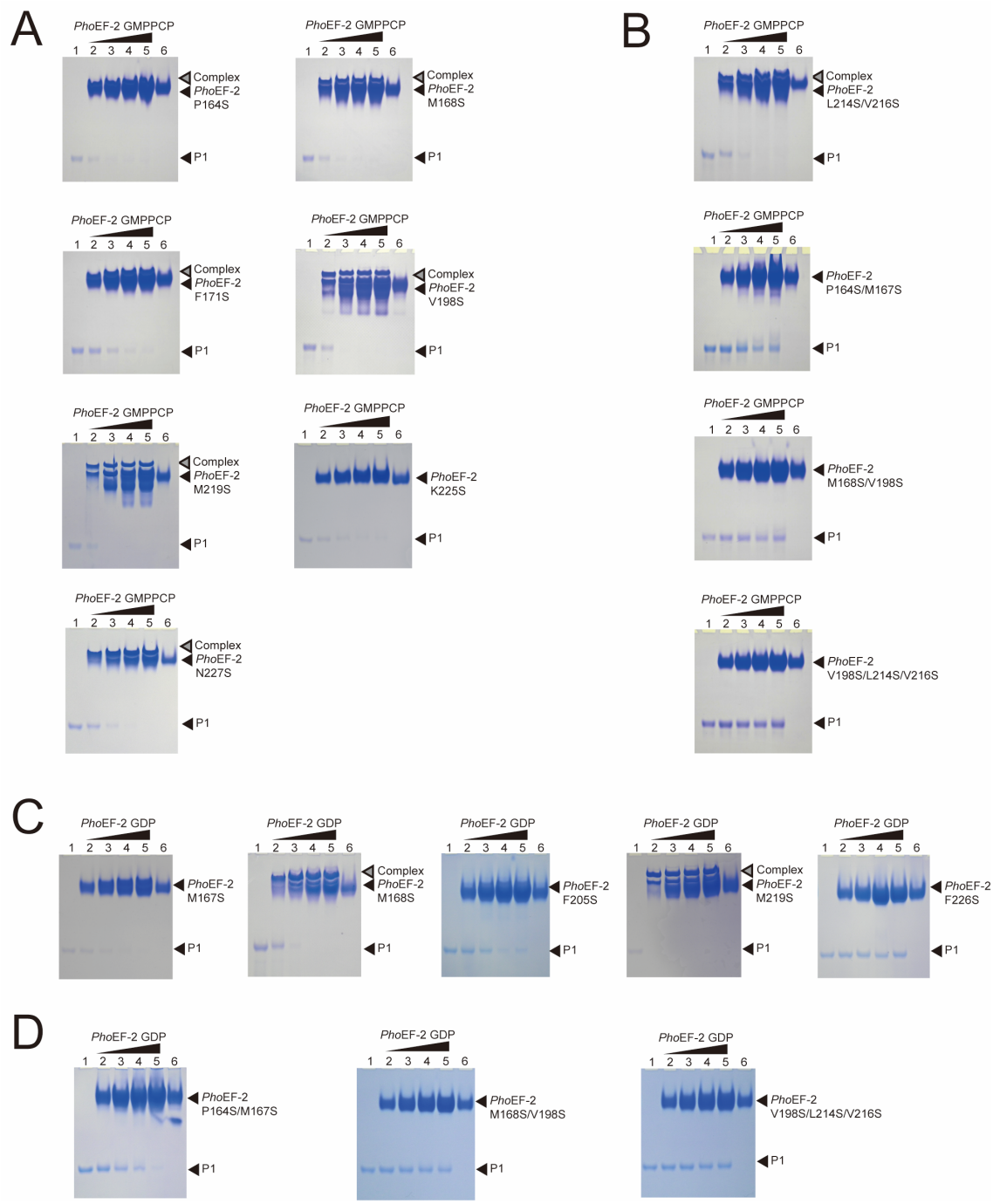

Figure S7. P1-binding assay of GMPPCP and GDP-bound *Pho*EF-2 mutants using Native-PAGE. (**A**) Binding assays between P1 and the *Pho*EF-2-GMPPCP point mutants P164S, M168S, F171S, V198S, M219S, K225S, and N227S. (**B**) Binding assay between P1 and the *Pho*EF-2-GMPPCP plural points mutants L214S/V216S, P164S/M167S,

M168S/V198S, and V198S/L214S/V216S. (**C**) Binding assays between P1 and the *Pho*EF-2-GDP point mutants M167S, M168S, F205S, M219S, and F226S, which may be key residues involved in the interaction with P1C11. (**D**) Binding assays between P1 and the *Pho*EF-2-GDP plural points mutants P164S/M167S, M168S/V198S, and V198S/L214S/V216S. The P1 homodimer (100 pmol) was incubated without the *Pho*EF-2 mutants (lane 1), or with 100 pmol (lane 2), 200 pmol (lane 3), 300 pmol (lane 4), or 400 pmol (lane 5) of the *Pho*EF-2 mutants in a 10 μL solution at 70 °C. Each *Pho*EF-2 mutant (100 pmol) was also incubated without P1 (lane 6).

Figure S8

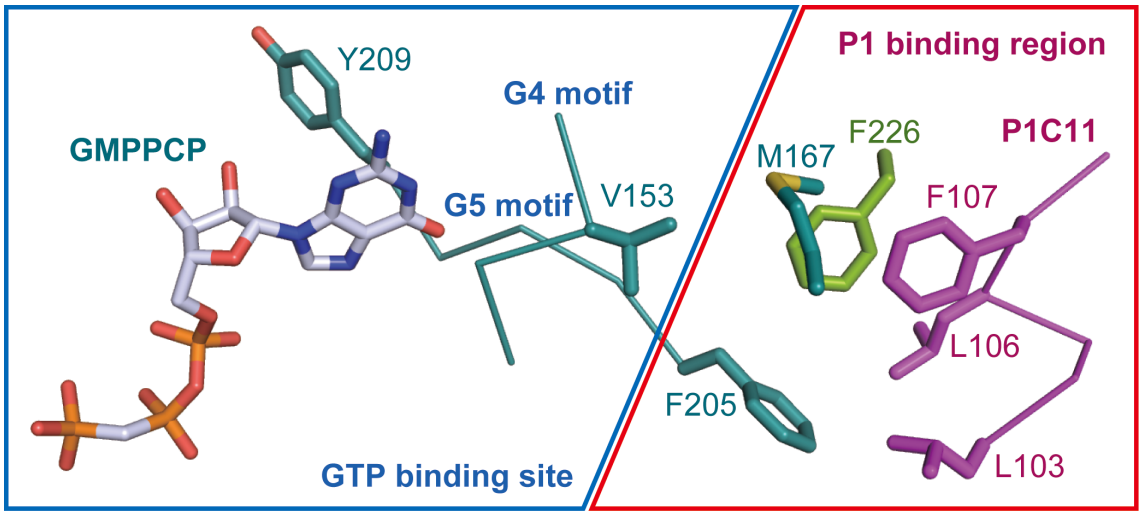

Figure S8. Structural relationship between the P1 binding region and GTP binding site of *Pho*EF-2-GMPPCP-P1C11. The color-coding is the same as used in Figure 3A. The main chain and side chains are represented by line and stick models, respectively. The GTP binding site and P1 binding region are shown as dark-blue and red boxes, respectively.

Figure S9

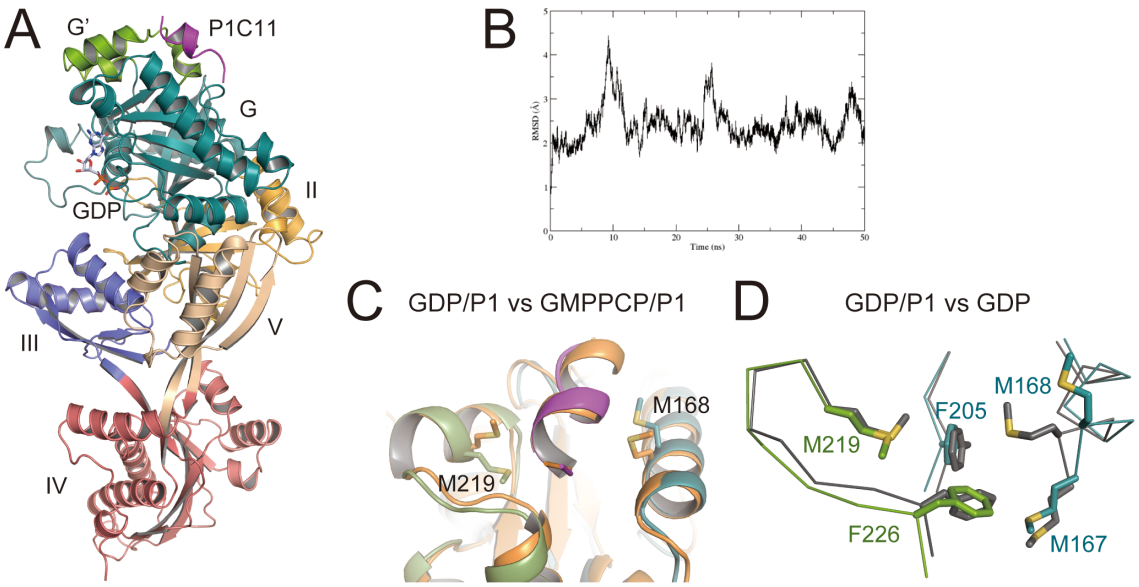

Figure S9. The molecular dynamics (MD) simulation model of GDP-bound *Pho*EF-2 in the presence of P1C11 (*Pho*EF-2-GDP-P1C11). (**A**) Overview of the MD simulation model. *Pho*EF-2-GDP-P1C11 is colored in the same way as in Figure 3A. (**B**) MD simulation trajectory of *Pho*EF-2-GDP-P1C11, in which the vertical axis is the root mean square deviation (RMSD) (Å) and the horizontal axis is the simulation time (ns). The RMSD of *Pho*EF-2-GDP-P1C11 was calculated as described previously (6). The energy of *Pho*EF-2-GDP-P1C11 was minimized and simulated for 50 ns to analyze how the structure of *Pho*EF-2-GDP responds to the presence of P1C11. The RMSD of the simulation was measured to determine the time at which the simulation was stable. Following an initial increase of approximately 3–4 Å in the RMSD, *Pho*EF-2-GDP-P1C11 stabilized at 15 ns. (**C**)–(**D**) Structural comparison of the P1C11-binding groove between the MD simulation model and crystal structures of *Pho*EF-2-GMPPCP-P1C11 (orange) (**C**), *Pho*EF-2-D2-GDP (gray) (**D**) by superposing P1-binding region. The side chains of important residues are represented by stick models, and the main chains are represented by ribbon and line models, respectively. S atoms are colored yellow.

Figure S10

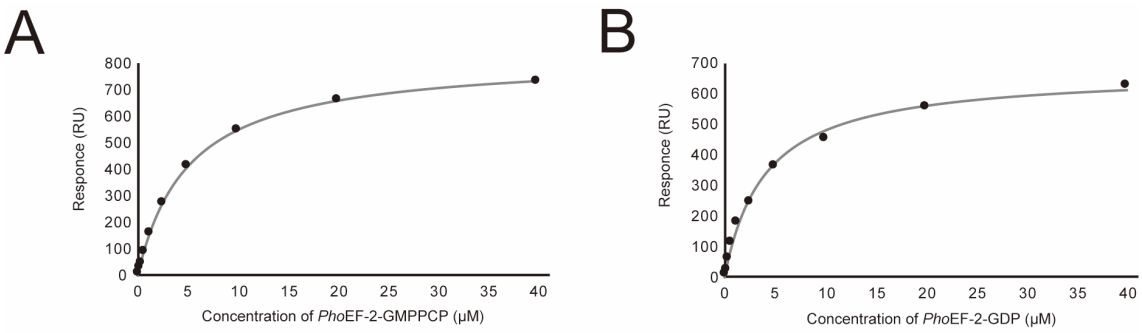

Figure S10. P1-binding assay of *Pho*EF-2-GMPPCP and *Pho*EF-2-GDP by SPR technique. The binding affinities were measured using BIACORE 3000 instrument. The K_D values of *Pho*EF-2-GMPPCP and *Pho*EF-2-GDP vs P1 were estimated to be 5.06 μM (**A**) and 4.05 μM (**B**), respectively.

Figure S11

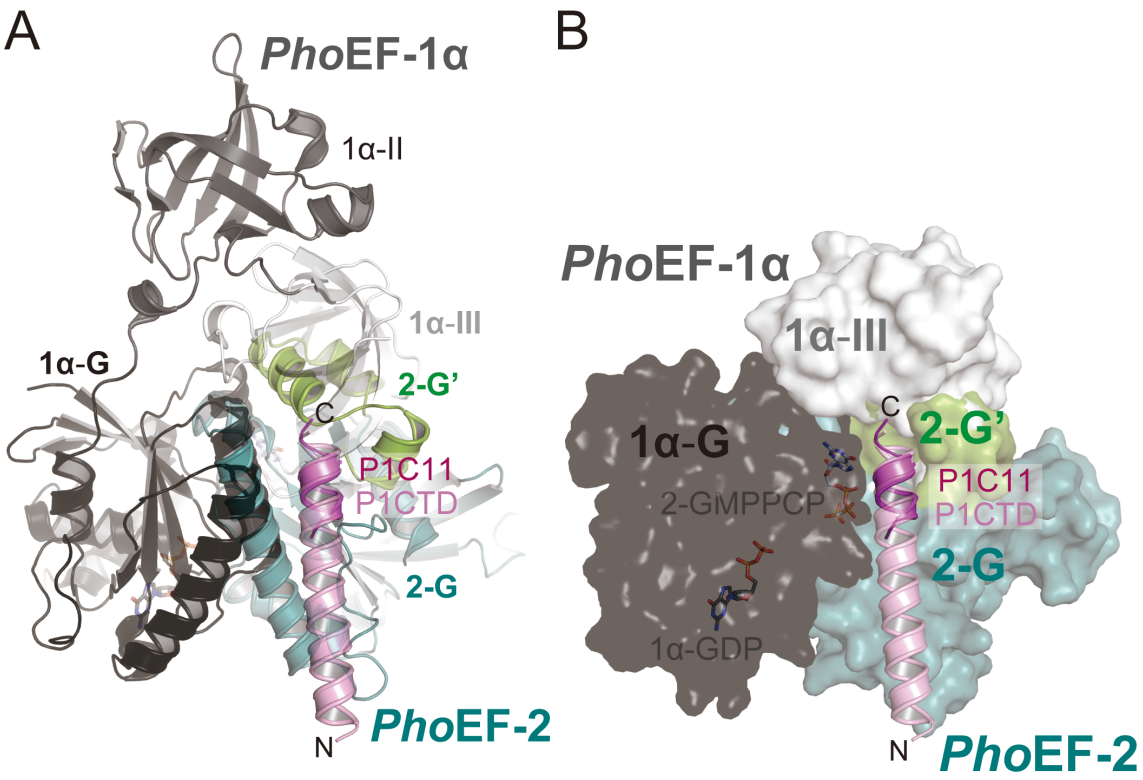

Figure S11. Structural comparison between GDP-bound *Pho*EF-1α in a complex with P1CTD (*Pho*EF-1α-GDP-P1CTD) (PDBID: 3WY9) and *Pho*EF-2-GMPPCP-P1C11. (**A**) *Pho*EF-1α-GDP-P1CTD superposed on *Pho*EF-2-GMPPCP-P1C11 by arranging P1C11. (**B**) Closed view of the P1-binding groove between *Pho*EF-1α (domains G and III) and *Pho*EF-2 (domain G and subdomain G′). These domains and GDP/GMPPCP are represented by surface and stick models, respectively. Domain G and subdomain G' of *Pho*EF-2-GMPPCP-P1C11 are colored in the same way as in Figure 3A, while domains G, II, and III of *Pho*EF-1α are colored black, gray, and white, respectively.

Figure S12

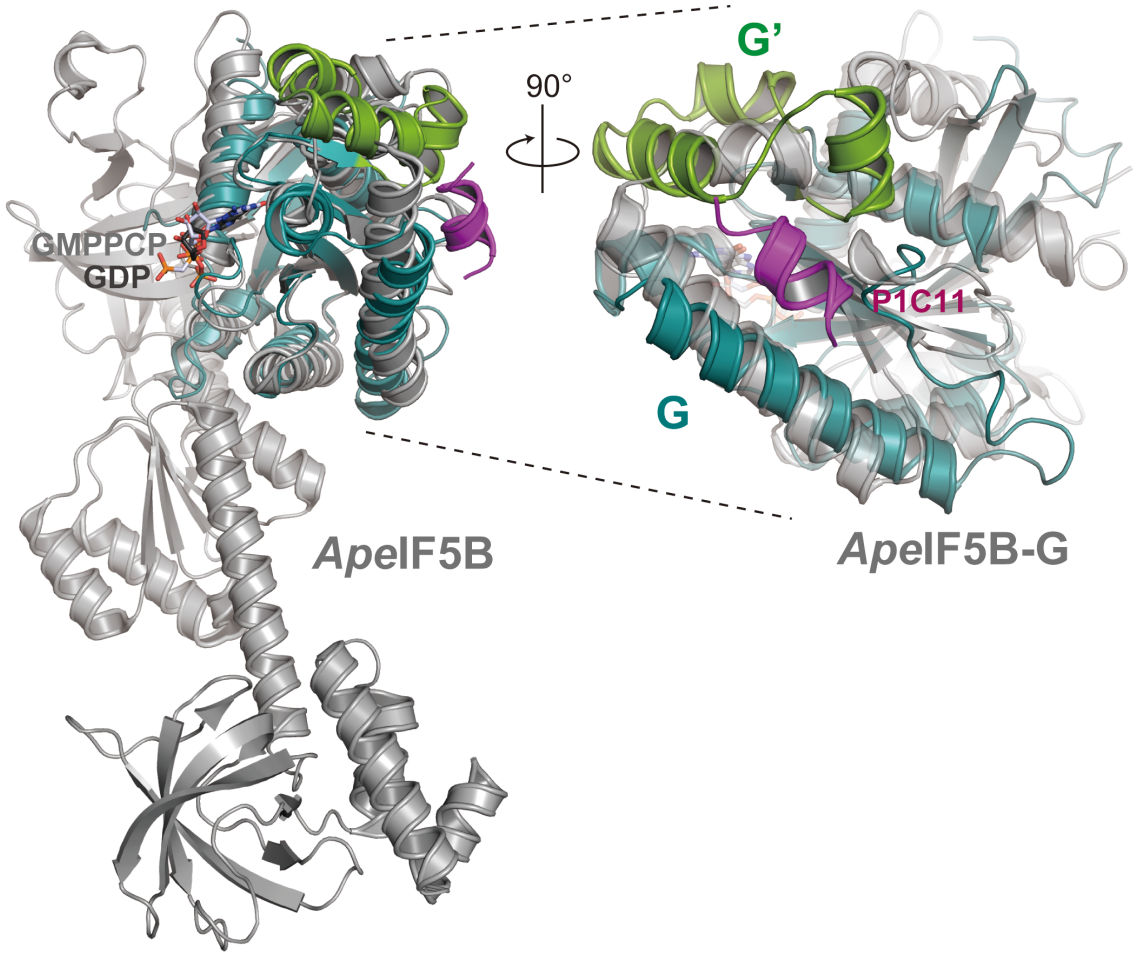

Figure S12. Structural comparison between aIF5B and *Pho*EF-2-GMPPCP-P1C11 without domains II–V. Domain G of aIF5B from *Aeropyrum pernix* (*Ape*IF5B-GDP; PDBID: 5FG3) (gray) was superposed on that of *Pho*EF-2-GMPPCP-P1C11, which is colored in the same way as in Figure 3A. The GDP in *Ape*IF5B and GMPPCP in *Pho*EF-2-GMPPCP-P1C11 are shown in the stick model.

Figure S13

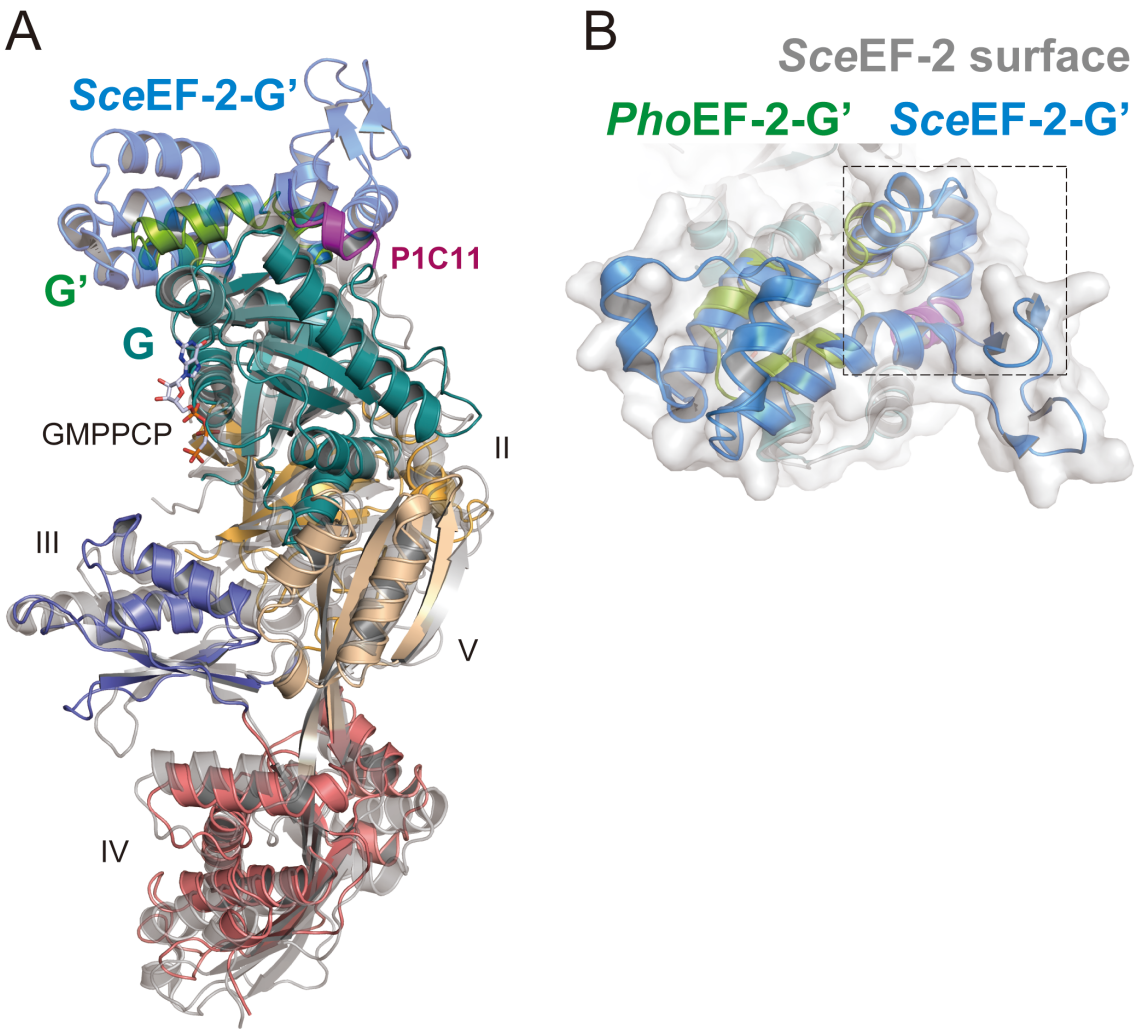

Figure S13. Structural comparison between eEF-2 and *Pho*EF-2-GMPPCP-P1C11. The subdomain G′ of *Sce*EF-2-Apo (PDBID: 1N0V) is colored blue and the other domains are colored gray. *Pho*EF-2-GMPPCP-P1C11 is shown in the same color as in Figure 3A. *Sce*EF-2 is represented by cartoon models. (**A**) Structural superposition of domain G between *Sce*EF-2-apo and *Pho*EF-2-GMPPCP-P1C11. (**B**) Top view of (A) of domain G and subdomain G′ with the molecular surface of *Sce*EF-2 colored in white.

Figure S14

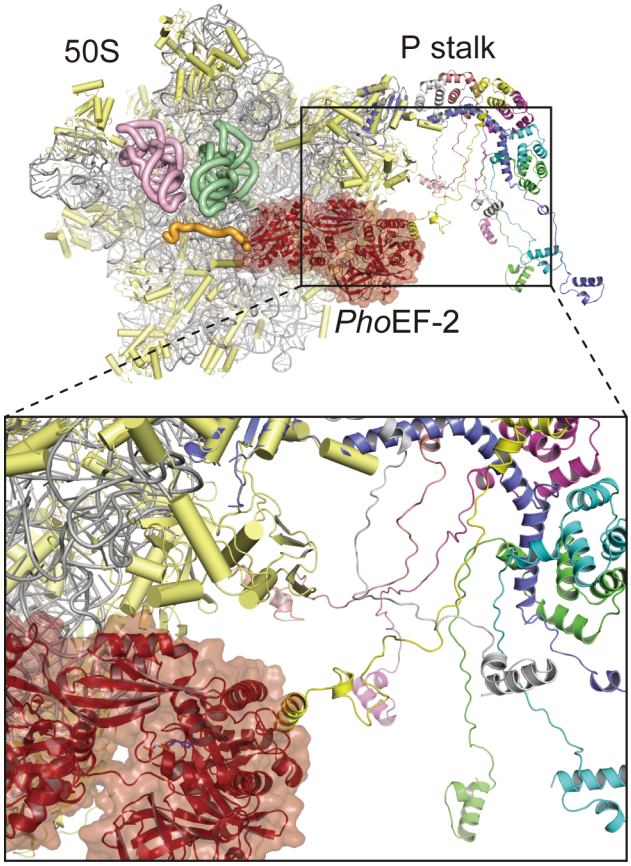

Figure S14. A model of aEF-2 recruitment by the ribosomal P stalk on the ribosome. The crystal structures of *Pho*EF-2-GMPPCP-P1C11 and P stalk P0-$[P1]_2[P1]_2[P1]_2$ (PDBID: 3A1Y) (12) are superposed on the large subunit of *Pyrococcus furiosus* ribosome (PDBID: 3J2L, 3J20 and 3J21) (top). The rRNA (gray), ribosomal proteins (yellow), and P stalk are represented in the ribbon model. EF-2 (red) is represented in both the ribbon and surface model. The tRNAs at the E/P site (pink) or P/A site (green), and mRNA (orange) are represented in the ribbon model. A close-up view is shown at the bottom.